Thin Solid Films 683 (2019) 156–164

Contents lists available at ScienceDirect

Thin Solid Films

journal homepage: www.elsevier.com/locate/tsf

Effect of NaF pre-cursor on alumina and hafnia rear contact passivation layers in ultra-thin Cu(In,Ga)Se_2 solar cells

Dorothea Ledinek*, Jan Keller, Carl Hägglund, Wei-Chao Chen, Marika Edoff

Uppsala University, The Ångström Laboratory, Department for Engineering Sciences, Division for Solid State Electronics, Box 534, 751 21 Uppsala, Sweden

ARTICLE INFO

Keywords:
Alkali
Alumina
Copper indium gallium diselenide
Hafnia
Passivation
Sodium fluoride
Ultra-thin

ABSTRACT

In this work, we evaluate the effect of NaF layers on the properties of Al_2O_3 and HfO_2 rear contact passivation layers in ultra-thin Cu(In,Ga)Se_2 solar cells. The 6 nm thin passivation layers were deposited by atomic layer deposition and neither intentionally opened nor nano-patterned in any extra-fabrication step. NaF layers, 7.5 or 15 nm thin, were deposited as precursors prior to CIGS absorber co-evaporation. The 215 nm thick absorbers were co-evaporated with constant evaporation rates for all elements. Directly thereafter, a 70 nm thick cadmium sulfide layer was deposited. Photoluminescence measurements indicate a strongly reduced recombination at the rear contact for all passivated samples compared to an unpassivated reference. Although the sample with Al_2O_3 passivation and a 15 nm NaF precursor layer luminesces by far the least of the passivated samples, solar cells made from this sample show the highest efficiency (8.6% compared with 5.6% for the reference with no passivation). The current-voltage curves of the solar cells fabricated from the sample with 7.5 nm NaF on top of the Al_2O_3 layer and both samples with HfO_2 exhibit blocking behavior to various degrees, but a high photoluminescence response. We conclude that NaF precursor layers increase conduction through the Al_2O_3 layer, but also reduce its effectiveness as a passivation layer. In contrast, conduction through the HfO_2 passivation layers seem to not be influenced by NaF precursor layers, and thus requires nano-patterning or thinning for conduction.

1. Introduction

Thinning down the Cu(In,Ga)Se_2 (CIGS) absorber decreases material consumption and thus the energy pay-back time and can increase throughput in production. It can also increase the open-circuit voltage (V_{OC}) if its disadvantages can be mitigated: It reduces photo-absorption, increases the impact of interface recombination on the collection function, increases voltage-dependent photocurrent collection and shunt like behavior under illumination (the superposition principle may fail) [1–5]. To increase absorption, the rear contact region has been modified by introducing reflection promoting oxide layers, light-scattering nanoparticles and nano-patterns [6–11]. Interface recombination has been curbed by front [12,13] and rear surface oxide passivation layers. If some or all of these strategies are successful, the free electrons and holes are confined to a smaller absorber volume compared to common absorber volumes, so that their concentrations and thereby the difference between their respective quasi-fermi levels increases. This, in turn, can lead to a higher V_{OC} in these optimized ultra-thin solar cells than in solar cells with thicker CIGS layers.

Generally, recombination at the absorber interfaces can be suppressed by changing the interface trap density (chemical passivation) and/or by making one carrier concentration much smaller than the other (carrier population control [14]). At a fixed difference in electro-chemical potential ε_{FC} - ε_{FV} between the quasi-fermi levels of the electrons (ε_{FC}) and holes (ε_{FV}) the Shockley-Read-Hall recombination rate is highest for equal hole and electron densities ($p = n$), and decreases strongly for asymmetric carrier densities [14,15].

The relative charge carrier concentration can be modified by 1) heavy doping (for example a p + rear contact layer in p-type crystalline Si solar cells [15,16]), 2) grading of the conduction band (for example through Ga grading with higher Ga concentration at the rear contact in CIGS solar cells [3,17,18]), 3) adjusting the work function of the metal contact so that majority charge carriers are accumulated [15] and 4) by other charge assisted control [14,15] (for example oxide charges in passivation layers).

If the passivation layer has a high concentration of negative charges, an accumulation layer - with strongly elevated hole concentration and reduced electron concentration - is formed in the surface region of an adjacent p-type semiconductor such as CIGS. A sufficiently high positive oxide charge, on the other hand, forms an inversion layer, with a

* Corresponding author.
E-mail addresses: dorothea.ledinek@angstrom.uu.se (D. Ledinek), jan.keller@angstrom.uu.se (J. Keller), carl.hagglund@angstrom.uu.se (C. Hägglund), chen.wei-chao@angstrom.uu.se (W.-C. Chen), marika.edoff@angstrom.uu.se (M. Edoff).

https://doi.org/10.1016/j.tsf.2019.05.024
Received 1 November 2018; Received in revised form 5 April 2019; Accepted 7 May 2019
Available online 08 May 2019
0040-6090/

high concentration of electrons and a low concentration of holes. In addition, the layer with strongly asymmetrical carrier concentrations acts as a carrier selective membrane as the charge carrier conductivities $\sigma_e = q{\cdot}\mu_n{\cdot}n$ and $\sigma_p = q{\cdot}\mu_p{\cdot}p$ and thus the charge carrier currents $J_n = (\sigma_n/q)(d\varepsilon_{FC}/dx)$ and $J_p = (\sigma_p/q)(d\varepsilon_{FV}/dx)$ become much larger for the majority carriers, even in the presence of a strong driving force $d\varepsilon/dx$ on the minority carriers close to the contact. Single carrier conduction and a reduction of interface recombination thus go hand in hand [15,19,20].

A large variety of oxides have been studied for passivation or reflection purposes in CIGS solar cells, including TiO_2 [21], SiO_2 [7,22,23] and ZnO [24] at the rear contact and Ga_2O_3 [13], Al_2O_3 [12], SiO_x and Si_3N_x [25] at the front contact. The most commonly investigated rear contact passivation layer material is, however, atomic layer deposited ALD-Al_2O_3. It has been shown to increase solar cell efficiencies for both c-Si and CIGS solar cells, which has be ascribed to both its oxide charge and its reduced interface trap density [26,27]. Both, negative and positive charges[25–28], have been observed in Al_2O_3 layers deposited by ALD on top of CIGS. In the latter case, the oxide charge can become negative after an anneal[26,28]. As the Al_2O_3 layer is exposed to a relatively high temperature during CIGS deposition as well, it probably has a negative charge as a rear contact passivation layer [26].

Hafnia (HfO_2) has also been considered for the rear contact passivation of solar cells, such as crystalline Si[28–32], organic solar cells [33], and recently for the front passivation of CIGS solar cells [25]. It has a higher refractive index of 2.09 compared to 1.66 for Al_2O_3 [34]. Its bandgap of 5.3 eV is somewhat lower than that of Al_2O_3 at 6.5 eV. Its valence band edge is 0.83 eV higher and its electron affinity 0.43 eV larger compared to Al_2O_3 [35]. The effectiveness of ALD-HfO_2 as a passivation layer on c-Si and the sign of its charge depend on several factors, including the cleaning method [32], ALD precursor, deposition temperature and process conditions [32], the post-deposition annealing method [28] and even illumination [32]. Therefore, the properties and function of HfO_2 as a passivation layer in CIGS solar cells cannot be adequately deduced from the existing literature.

As all the previously mentioned oxide passivation layers are electric insulators, they have been nano-structured to maintain a good contact between the absorber and the rear contact. On CIGS solar cells the nanostructures include point contacts and line contacts [9,36]. Nanosphere shaped cadmium sulfide (CdS) particles precipitated during chemical bath deposition (CBD) [37–39] have been used in lift-off processing, and Mo nano-particles forming contacting points [10], electron-beam lithography [40,41], photo-lithography [7,9,36], laser-interference lithography [22] and nano-imprint lithography [21] have been used to open up the passivation layers. Even a self-organized spray-pyrolysis based process has been applied to deposit porous Al_2O_3 onto the transparent SnO_2:F rear-contact [42].

While the effects of Na on CIGS absorbers are well known (even if not comprehensively explained), its effects on the passivation layers themselves has not been studied in detail. For example, Vermang et al. [37,38] conclude that 2 and 5 nm thick Al_2O_3 passivation layers do not conduct current in the completed solar cells and that point contacts are required in the passivation layers, by comparing rear passivated samples without NaF precursor and without nano-patterning with a rear passivated sample with NaF precursor and nano-patterning. In contrast, we showed in a previous study [43] that using a NaF precursor layer on top of < 7 nm thin Al_2O_3 rear contact passivation layers can increase the conduction through the Al_2O_3 passivation layers sufficiently to make the extra-fabrication step of opening up the passivation layer unnecessary. However, the CIGS layer thickness in that work was 1 µm and therefore the influence of the passivation on the device characteristics small. In this work, we thin the absorber layer down to only 215 nm and compare the impact of NaF on Al_2O_3 passivation layers with its impact on HfO_2 passivation layers. By thinning the absorber layer down, the influence of the recombination at the rear contact on the effective minority carrier life-time is increased, making it more accessible to photoluminescence (PL) measurements.

2. Photoluminescence theory

Spectral PL has been used to characterize chalcogenide and kesterite thin films with and without passivation layers. Passivation layers applied on top of the absorber layer increase the PL intensity [44–46]. However, as these passivation layers have not undergone the heat-treatment and Se atmosphere during CIGS processing, they are not representative for the passivation layers at the rear contact in a substrate structure [46]. To get samples that are more representative of an actual rear contact, Joel et al. [46] built a “rear” PL structure of soda-lime glass/Mo/Al_2O_3/CIGS/CdS to be illuminated through the glass. To achieve transparency, these samples had an only 10 nm thin Mo rear contact, which would lead to a high series resistance for completed solar cells. To make the PL results and the solar cell characteristics directly comparable in this study, we attempt to measure spectral PL and then to complete the solar cell processing to additionally characterize the completed solar cells. Only recently, Salomé et al. [47] compared the PL signals measured on completed unpassivated and passivated CIGS solar cells with a 350 nm thick absorber and found a larger width of the PL peak for the unpassivated cells, but they were cautious and did not report intensities due to different optical alignments within the cells. Generally, PL intensities are very low, if measured on completed CIGS solar cells with a ZnO/ZnO:Al layer. As the full stack of window layers induces a much stronger electric field in the CIGS than with only the CdS layer, it separates the charges fast and efficiently [48], so that the radiative recombination rate is strongly reduced. Therefore, we measure on samples with only a CdS buffer layer but without ZnO/ZnO:Al window layers on the absorber.

The differential photon current density dI, i.e. the number of photons with an energy $\hbar\omega$ per unit area and time emitted from the surface of a semiconductor into the environment, depends exponentially on the difference of the quasi-fermi levels of electrons and holes according to [19].

$$dI = a(\hbar\omega)e^{\frac{\varepsilon_{FC}-\varepsilon_{FV}}{kT}}\frac{\Omega}{4\pi^3c^2}\frac{(\hbar\omega)^2}{e^{\frac{\hbar\omega}{kT}}-1}d(\hbar\omega) = a(\hbar\omega)\,e^{\frac{qV_{OCmax}}{kT}}\frac{\Omega}{4\pi^3c^2}\frac{(\hbar\omega)^2}{e^{\frac{\hbar\omega}{kT}}-1}d(\hbar\omega) \quad (1)$$

Eq. (1) is the Boltzmann approximated version of Planck's generalized law. The absorptance a($\hbar\omega$) is a a function of the layer thicknesses and the materials used in the sample stack and $V_{OCmax} = 1/q\ (\varepsilon_{FC} - \varepsilon_{FV})$ is the maximally extractable V_{OC}. Ω is the solid angle, c the velocity of light, $\hbar$ the reduced Planck constant, k the Boltzmann constant and q the elemental charge. As this equation was derived with the help of the Boltzmann approximation of the Fermi distribution, it is only valid for non-degenerate semiconductors. In contrast to Planck's law, they do not need to be black and can have different Fermi distribution for electrons and holes over states, as is the case in illuminated semiconductors. As $e^{\frac{\varepsilon_{FC}-\varepsilon_{FV}}{kT}} = \frac{p\cdot n}{n_i^2}$, with the intrinsic carrier concentration n_i, dI is proportional to the number of free charge carriers. As non-radiative recombination reduces those concentrations and the fermi-level splitting, a low PL intensity indicates high non-radiative recombination rates. For semiconductor samples with a similar sample stack, as in the case for our samples, the difference in V_{OC} between two samples can thus be estimated from two measured PL intensities I_1 and I_2 at a fixed wavelength according to

$$\Delta V_{OC,PL} = \frac{kT}{q}\ln\frac{I_1}{I_2} \quad (2)$$

3. Sample preparation

Five samples with 12 solar cells each were produced: a reference sample, two samples with an Al_2O_3 passivation layer and two with a HfO_2 passivation layer between the sputtered Mo rear contact and the co-evaporated CIGS absorber layer. The passivation layers were deposited by ALD to a thickness of 6 nm. A 7.5 or 15 nm thick NaF precursor layer was evaporated onto the passivated rear contacts prior to absorber co-evaporation. During the NaF deposition the samples were not intentionally heated and the source sample distance was around 0.5 m. The samples are referred to according to their passivation and pre-cursor layer thicknesses as “baseline reference”, “7.5NaF6Al”, “15NaF6Al”, “7.5NaF6Hf” and “15NaF6Hf”, respectively. The CIGS layers were produced in one single co-evaporation run. During the first 500 s of the co-evaporation run the substrate temperature was raised from room temperature to 410 °C. At the time $t = 1600$ the shutter was opened and at $t = 1730$ s the temperature was raised to 530°C. At $t = 1900$ the shutter was closed and the substrate heater switched off. Thus, the samples were preheated at 410 °C for 18 min before the evaporation started, after which they were deposited during 2 min at 410 °C and during 3 min at 530 °C with a temperature ramp of approximately 1 min in between. The samples cooled down in vacuum to less than 100°C in about two hours and are unloaded. The resulting CIGS layer has flat elemental profiles with a GGI = [Ga]/([Ga] + [In]) of about 0.15 and a CGI = [Cu]/([Ga] + [In]) of about 0.80 as determined by XRF, calibrated with a CIGS calibration sample. The absorber thickness was measured to 215 nm by transmission electron microscopy (TEM) and profilometer analysis. The flat elemental profiles are used to exclude additional rear surface passivation and selective conductance by Ga grading. Apart from a shortened CIGS evaporation time to thin down the absorber and for exchanging mechanical scribing of the cells to photolithography-assisted etching, we used the same procedures for the sample preparation as in our previous work [43]. In another previous experiment, four samples with 13 nm thick passivation layers and another baseline reference were produced, but reliable measurement results cannot be presented as the CIGS layers peeled from the passivation layer on three of them. With 6 nm oxide layers, peeling was not a problem. We emphasize that all solar cell processing was the same for both solar cell samples, apart from the passivation layers and the use of a NaF precursor.

As the atomic layer deposition of HfO_2 and photolithography are new in this article, they merit a closer description. With decreasing absorber thickness, the likelihood that mechanical scribing introduces shunts at the edges of the cells increases. Therefore, it is replaced by photolithography assisted etching. The cell layout and the size of 0.5 cm^2 remains unchanged. The samples are coated with 2 µm positive photoresist (AZ®9260 photoresist, AZ Electronics Materials) and spun at 6000 rpm (Karl Süss LabSpin6/8) for 40 s. Thereafter, the samples are pre-baked at 115 °C for 120 s, exposed through a double-sided aligner (Karl Süss MA6/BA6) with light with a wavelength between 365 nm and 405 nm. They are baked again at 115 °C for 300 s and developed with a 20% diluted developer (AZ 400 k). Finally, the unpassivated window layer is etched in 1 M HCl solution for 60 s and the photoresist is removed by acetone solution.

HfO_2 was grown by atomic layer deposition (ALD) in a hot wall, viscous flow reactor (Picosun R200), from tetrakis(dimethylamino) hafnium(IV) (TDMAH, Sigma Aldrich) and water precursors. The substrate was kept at a temperature of 170 °C while the TDMAH source container was kept at 63 °C, similar to previous work using these precursors [49]. A pulse/purge sequence of 0.2/10/0.1/10 s was employed for the TDMAH/H_2O cycle. Based on in situ spectroscopic ellipsometry (Woollam RC2, using wavelengths from 300 to 1690 nm), a linear growth rate of 1.2 Å/cycle was observed, in agreement with the HfO_2 thickness deduced from TEM imaging. To deposit the Al_2O_3 layers, trimethylaluminum (TMA) and water were used as reactants in a temporal Picosun Sunale R200 ALD system at 300 °C. The growth rate is known to be 0.9 Å/cycle [43]. To achieve close to 6 nm layer thicknesses, 50 ALD cycles were used for HfO_2 and 70 cycles were used for Al_2O_3.

4. Sample characterization

On all samples, photoluminescence (PL) was measured at room temperature in a Renishaw inVia confocal Raman microscope after the chemical-bath deposition of the CdS buffer layer, but before the sputtering of the i-ZnO/ZnO:Al window layer to mitigate the charge separation effect [48]. On every sample, five random measurement spots were selected and illuminated by a 785 nm continuous wave laser at a power of 0.07 µW and a spot size of about 20 µm. An InGaAs photodetector was used to measure the PL response between 0.81 and 1.55 eV. The data was integrated over the whole spectrum, which essentially consisted of a single broad PL peak centered at about 1.08 eV.

The reflectance of whole cell stacks was measured with a Perkin Elmer L900 spectrophotometer with an integrating sphere. The current-voltage set-up was first calibrated with the short-circuit current density (J_{SC}) of a calibration Si-based solar cell. During the data analysis, the J_{SC} was corrected for spectral mismatch between the ELH lamp and the AM1.5G spectrum by a reduction of 6 to 8% using the photocurrent calculated from external quantum efficiency (*EQE*) measurements at ambient light on three cells per sample. The fill-factor and the V_{OC} were not adjusted. More details on the current-voltage and the *EQE* measurement-set up can be obtained from previous articles [4,41,43,50].

The optical constants and thicknesses of the different materials of the stack were determined by spectroscopic ellipsometry. Layers were measured before additional layers were deposited on top, on samples prepared under similar conditions as those used here. Rough interfaces were taken into account by means of Bruggeman effective medium theory, with the filling factor, depolarization and layer thickness as fitted parameters. The various measurement sets (3 angles of incidence, wavelengths from 260 to 1690 nm, for each interface) were combined in a multi-sample analysis, to consistently determine all properties of the stack. Once the optical properties and layer thicknesses were established, the transfer matrix method was used to calculate the absorption in each layer. An estimate for the photocurrent was finally obtained by integrating the absorptance in the CIGS layer over wavelengths and assuming 100% collection efficiency.

The transmission electron microscopy (TEM) cross section samples were prepared with a dual beam focused ion beam and scanning electron microscope (FIB-SEM, FEI Strata DB235). The samples were attached to a Ti grid and thinned to electron transparency. For TEM analysis, a probe corrected FEI Titan Themis operated at 200 kV and equipped with the SuperX system for energy dispersive X-ray spectroscopy (EDX) was used. The STEM-EDX spectral images were acquired and evaluated with the Esprit software provided by Bruker.

5. Results and discussions

5.1. Photoluminescence measurements

The arithmetic averages and standard deviations of the integrated PL intensities for all samples are summarized in Fig. 1. The PL intensities are a factor 55–760 larger for the passivated samples compared to the unpassivated reference. According to the logarithmic relation (Eq. (2)) between the V_{OC} and the PL intensities, the estimated gain $\Delta V_{OC,PL}$ due to the passivation layers lies between 100 and 170 mV.

For our solar cells, the attenuation depth is about equal to the absorber thickness (215 nm) for light with a wavelength of 785 nm traveling in CIGS with a GGI of 0.15 according to corresponding ellipsometry measurements and calculations as in our previous work [41]. Above this wavelength, light intensity will be found throughout the whole absorber layer, with a distribution that depends on coherent superposition of the forward propagating field with that reflected from

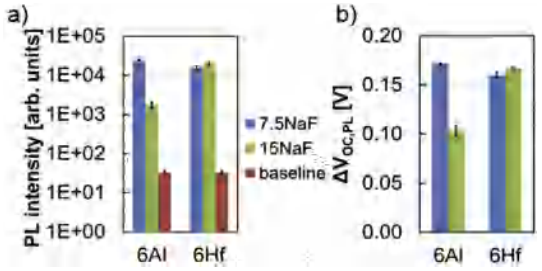

Fig. 1. a) Photoluminescence intensities for all investigated samples. b) Estimated open-circuit voltage gains $\Delta V_{OC,PL}$ of the passivated samples compared to the baseline reference.

the rear. The reflectance at the rear contact is, however, not dramatically different when a 6 nm Al_2O_3 layer is introduced between the Mo and CIGS according to modeling by the transfer-matrix method with ellipsometry determined optical constants for CIGS and Mo, and tabulated data for Al_2O_3. For example, it changes from 13% to 16% at 785 nm wavelength. Since most light will still be absorbed in a single pass of the absorber, the contributions to differences in the PL spectrum are relatively small due to these changes in rear reflectance. Furthermore, we can safely assume that the sum of the depletion region width and the bulk minority carrier diffusion length is larger than the absorber layer thickness on all samples, so that the effect of non-radiative recombination at non-passivated interfaces becomes very pronounced. Assuming that the interfaces at the front contact are not changed by the introduction of the passivation layers at the rear contact, the higher PL signal for the passivated samples indicates a larger quasi-fermi level splitting. Therefore, we conclude that both the Al_2O_3 and HfO_2 passivation layers reduce the recombination rate at the rear contact.

Interestingly, the PL intensity for the 15NaF6Al sample is nearly a factor 14 lower compared to the 7.5NaF6Al sample, which translates into a possible difference in $\Delta V_{OC,PL}$ = 70 mV according to eq. 2. On the other hand, the effect of the NaF thickness on the PL signal of the HfO_2 passivated samples is minor. The PL-intensity of the 15NaF6Hf sample is less than a factor 1.3 larger than that of the 7.5NaF6Hf sample, corresponding to a $\Delta V_{OC,PL}$ = 6 mV. Considering our small sample size and the standard deviations, we deem this difference as not significant. The $\Delta V_{OC,PL}$ of the 7.5NaF6Al sample is 5 and 11 mV larger than $\Delta V_{OC,PL}$ of the 15NaF6Hf and 7.5NaF6Hf samples, respectively.

We will discuss these PL results considering the *JV* (current density –voltage) results later. However, we can conclude here that the rear contact can be effectively characterized by PL measurements from the front, if a CdS layer is deposited on a thin enough absorber layer. This makes our method complementary to the rear PL structure suggested in [46]. For ultra-thin CIGS solar cells our method enables the fabrication of complete solar cells on the PL characterized samples, thus enabling a straight forward comparison between PL results and *JV* curves.

5.2. Current-voltage measurements

As can be seen in Fig. 2a and Fig. 3, the J_{SC} values for the samples with HfO_2 are close to zero regardless of NaF thickness. This indicates that the HfO_2 passivation layers block the photocurrent strongly. This result agrees with the findings of our pre-study (not shown here) with 1 µm thick absorber layers, in which the HfO_2 passivated samples blocked the current equally strongly no matter if 7.5 or 15 nm NaF precursor were used, or no precursor at all.

In contrast, the best cells on the Al_2O_3 passivated samples have a nearly 7 mA/cm^2 higher J_{SC} than the best cell on the reference sample. Our optical model for the stack indicates that the maximum gain in J_{SC} due to enhanced optical reflection for a CIGS/Al_2O_3/Mo stack compared to a CIGS/Mo stack with previously stated layer thicknesses is very low (0.3 mA/cm^2). to The result agrees well with previous

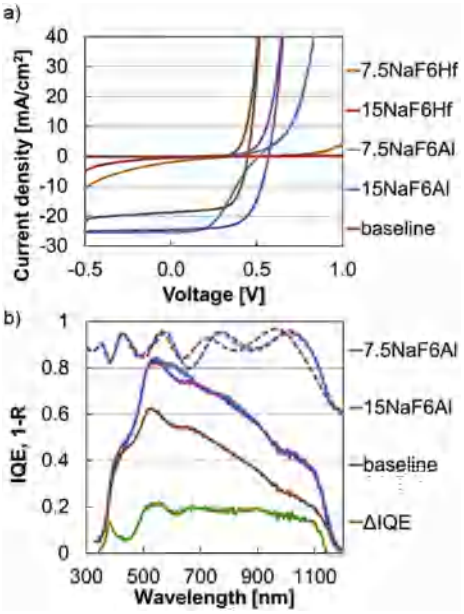

Fig. 2. a) Dark and light current density-voltage (*JV*) curves for the best cell of each sample. b) Dashed lines: 1-reflectance (1-R) of the whole solar cell stack. Sold lines (except green): Internal quantum efficiency (IQE), Green solid line: IQE difference between the 15NaF6Al sample, and the baseline reference. (For interpretation of the references to colour in this figure legend, the reader is referred to the web version of this article.)

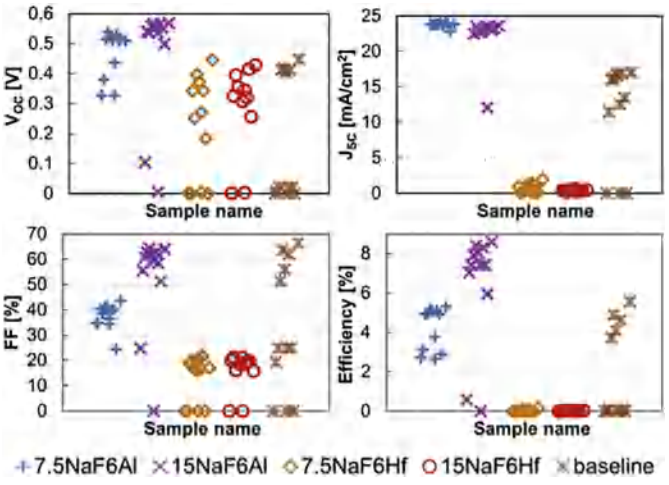

Fig. 3. Solar cell parameters short-circuit current density (J_{SC}), open-circuit voltage (V_{OC}), fill-factor and efficiency for all 12 cells on all samples.

calculations [47], and implies that the increased J_{SC} not only stems from optical effects, but to a significant degree also from the passivating effect of the Al_2O_3 layers.

The highest V_{OC} values on the 15NaF6Al sample exceed the highest V_{OC} on the reference sample by 120 mV, in approximate agreement with the estimation based on the PL data ($\Delta V_{OC,PL}$ = 103 ± 5 mV). This increase in V_{OC} for passivated cells also agrees qualitatively with simulation results [51], that predict such an increase for samples with absorber thicknesses smaller than the bulk diffusion length. The passivation layer then considerably enhances the collection efficiency for carriers generated close to the rear contact, and both the negative fixed charges and the lower interface trap density contribute to this enhancement. The *JV* curves of the cells on the 7.5NaF6Al sample suffer from a kink (compare Fig. 2), which reduces the fill-factor to max 45% and also reduces the V_{OC} due to the partial blocking of the photocurrent by about 40 mV compared to the V_{OC} of the 15NaF6Al sample. As a

difference in fermi-levels $V_{OCmax} = 1/q\ (\varepsilon_{FC} - \varepsilon_{FV})$ in the absorber bulk is only the maximum attainable V_{OC} that can be measured at ideal contacts, this reduction in V_{OC} does not contradict the $\Delta V_{OC,PL}$ obtained by the "contactless" PL measurements.

In the end, the efficiency of the best cell on the 15NaF6Al sample is 8.6%, corresponding to a gain of 3.0% (absolute) compared to the best cell efficiency (5.6%) of the reference sample. Despite the kink in the *JV* curves, the cells on the 7.5NaF6Al sample still reach about the same efficiency as the baseline reference sample due to their higher J_{SC}.

These *JV* results can be compared to similar experiments on ultra-thin CIGS solar cells but with a highly reflective rear contact [22]. CIGS solar cells were produced with a 190 nm thick, NaF post-deposition treated absorber, with a CGI ≈ 0.9 and a GGI ≈ 0.28 with and without a 60 or 130 nm thick SiO_2 rear contact layer that enhances the rear contact's reflectance. The researchers structured the layer with point contacts by photolithography and varied the pattern, the pitch, the size of contact openings and the opened-up area. The solar cells on their reference sample reached an efficiency of 5.9% and on their best point-contact sample 9.0%, a difference of 3.1% absolute, which is coincidentally similar to our results.

As previously observed for CIGS solar cells with thin and ultra-thin absorbers [4,21,39,40,47], the light *JV* curves of the unpassivated reference samples have larger values for the apparent shunt conductivity ($dJ/dV|_{V=0}$) than the light *JV* curves of the passivated samples. These large apparent shunts under illumination have been explained by voltage dependent current collection [52], but when quantifying this effect by biased quantum efficiency measurements and considering the shunt under dark conditions, a residual shunt in the light *JV* curve can still remain unexplained [4].

Voltage dependent current collection [4,47] takes place in devices with a low effective diffusion length, caused by either a low bulk minority carrier diffusion length or by rear contact recombination, in combination with negligible recombination in the space-charge region. The collected current is then dominated by carriers from the depletion region. When the solar cell is increasingly forward biased, the width of the depletion region is gradually reduced and hence, current collection is decreased. As seen in Fig. 2, even in this investigation, a residual shunt remains for the unpassivated reference cells; the slope of the dark curve between −0.4 and 0.1 V is 0.08 mS/cm^2 for a selected representative cell on the unpassivated baseline sample. It increases by a factor 46 to 3.7 mS/cm^2 under illumination. In contrast, the slope only doubles from 0.58 to 1.15 mS/cm^2 for a representative cell on the 15Naf6Al sample. To quantify the voltage-dependent current collection, we measured the quantum efficiency at −0.5 V (not shown) in addition to the measurements at 0 V (see Fig. 2b) and calculated $\Delta J/\Delta V$ to be 1.7 mS/cm^2 for one representative cell on the baseline reference and 1.0 mS/cm^2 for the 15Naf6Al sample. While the dark shunt together with the voltage-dependent current collection can completely explain the observed shunt-like behavior for the 15NaF6Al sample, a residual slope of 2 mS/cm^2 is left unexplained for the baseline reference. Since the passivation layer reduces not only voltage-dependent current collection by increasing the effective minority carrier diffusion length, but also extinguishes the residual shunt-like behavior in our ultra-thin devices, the residual ($dJ/dV|_{V=0}$) in the non-passivated case is concluded to be related to the rear contact.

Very few cells are severely shunted on the 7.5NaF6Al (0) and the 15NaF6Al (2) samples, compared to 7 cells on the baseline reference. We want to point out that the reference sample is not a bad outlier, as we have obtained an equal baseline sample with a similar number of shunted cells and efficiencies for another CIGS evaporation batch. Therefore, we conclude that an Al_2O_3 passivation layer may protect ultra-thin CIGS solar cells against shunting.

5.3. IQE characteristics

The reflectance spectra measured on the whole sample stack (see Fig. 2b) indicate that the Al_2O_3 passivation layer does not significantly increase the amount of light that is reflected at the rear contact and escapes the cell up to a wavelength of about 950 nm. This result is plausible, as a 6 nm Al_2O_3 layer only increases the reflectance at the rear contact by a few absolute percent. The difference in reflectance for the whole stacks between the two Al_2O_3 passivated samples lies within the measurement error.

In Fig. 2b, the EQE corrected by the external reflection - referred to as internal quantum efficiency *IQE = EQE/(1-R)* - is depicted. The interference pattern has not vanished completely between 500 and 600 nm, which could stem from misalignment between the EQE set-up and the photo-spectrometer or lateral inhomogeneities in the films, as the EQE and the reflectance were not measured on exactly the same spot on the sample and the light spot of the EQE set up is much smaller. The Al_2O_3 passivated cells reach a maximum IQE of over 80% for the passivated samples compared to 60% for the unpassivated reference. Between 500 nm and 1100 nm in wavelength the absolute difference in IQE between the 15NaF6Al sample and the baseline sample is nearly constant. These results are consistent with gains in collection efficiency in contrast to gains by enhanced light absorption, which would mostly occur for long wavelengths close to the band gap. Therefore, the EQE results confirm that the gain in J_{SC} stems mostly from passivation effects, and less from optical effects in agreement with earlier observations by us and others.

5.4. TEM investigation of the rear contact interfaces

In our previous work [43], a TEM EELS analysis indicated that NaF makes the Al_2O_3 porous and that GaO_x reduces the Al_2O_3 thickness locally. In this section we will compare the rear contact interfaces of the 7.5NaF6Al (slight blocking), 15NaF6Al (no blocking) and 15NaF6Hf (strong blocking) samples by means of STEM-EDX elemental mapping to compare the effect of NaF on the different passivation layers Fig. 4a shows a bright-field (BF) TEM image of a cross section of the 15NaF6Al sample. It reveals a roughly square geometry of the CIGS grains, with grain columns spanning the whole CIGS thickness connecting the front and the rear contact. EDX profiles of the whole cells (not shown) also

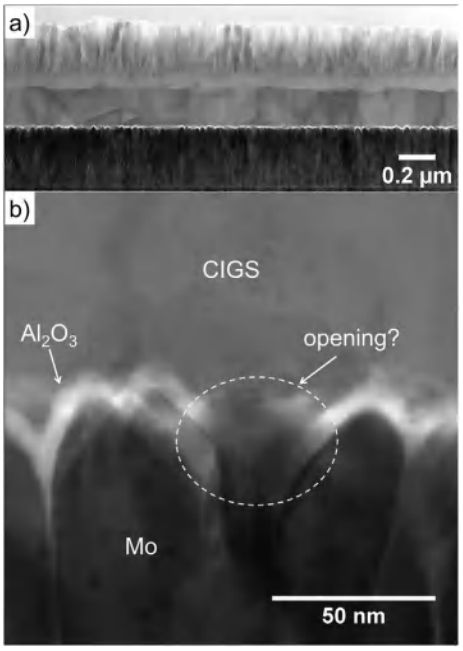

Fig. 4. Transmission electron microscopy (TEM) bright-field (BF) image of a) the whole solar cell stack of the 7.5NaF6Al and b) the rear contact region for the 15NaF6Al sample. On the left the Al_2O_3 layer is visible deep down in the grain boundaries of the Mo crystals.

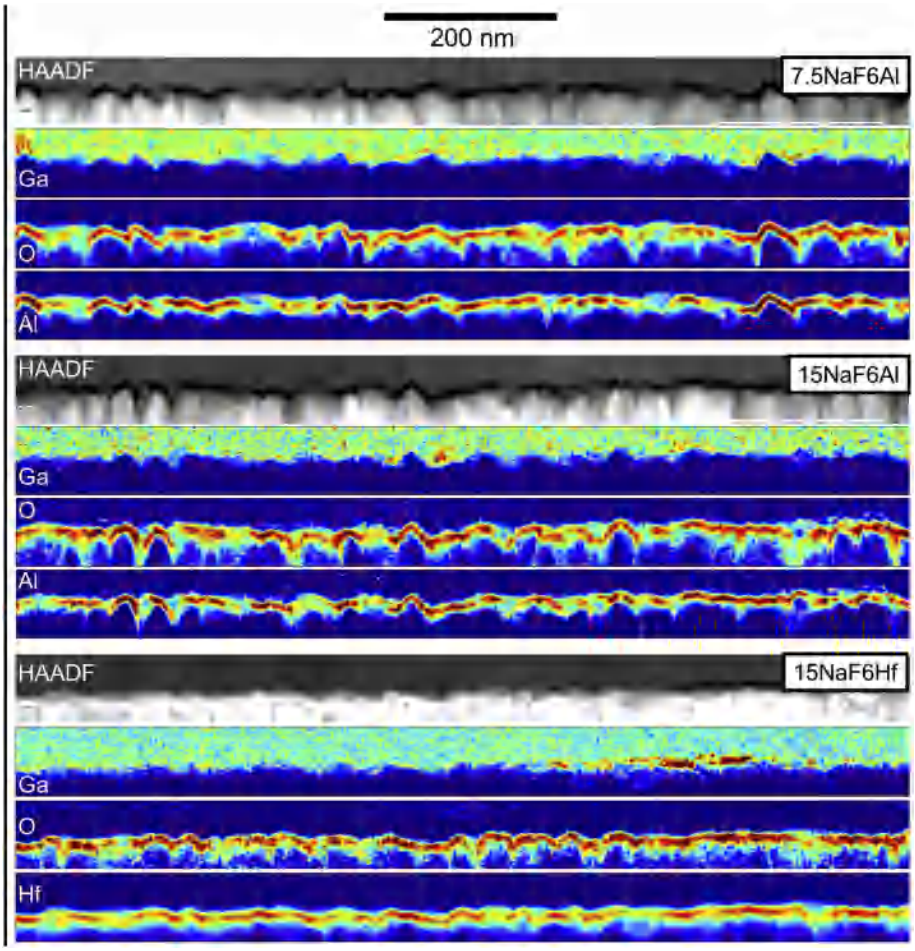

Fig. 5. Dark field image (HAADF) and energy dispersive x-ray spectroscopy (EDX) elemental maps for Al/Hf, O, Ga of the rear contact region for the 15NaF6Al, the 7.5NaF6Al and the 15NaF6Hf sample. The fiducial mark on the top is valid for all subfigures.

confirm that no gradients in Cu, In, Ga and Se exist in the CIGS absorber. Fig. 4b reveals that the ALD-Al_2O_3 grows predominantly conformally on Mo and evenly coats very narrow grooves in the surface topography (and maybe even grain boundaries). Locally however, the Al and O signals in the EDX maps are smeared out or interrupted (Fig. 5). It is further evident that the TEM lamellae (70 nm) are thicker than the Mo grains (30 nm), so that several Mo grains can shade each other. Thus, the alignment of the Mo grain boundaries has a large impact on the accessible information. Therefore, neither the TEM images in Fig. 4b) nor the quantified EDX maps in Fig. 5 are able to reveal if the passivation layers are closed and we do not find any clear difference between the 15NaF6Al and the 7.5NaF6Al sample. On the other hand, lowered Al and O concentrations can also indicate a thinning down of the Al_2O_3 layers. A reduction of the Al_2O_3 to 1–2 nm would already allow for a sufficient tunneling current [12,43,53].

To judge how much the surface roughness impairs the analysis, we compared the two Al_2O_3 passivated samples additionally with the 15NaF6Hf sample, where we deem that the existence of holes or tunneling contacts can be excluded according to the complete current blocking found in our *JV* results. Unfortunately, HfO_2 has a low contrast to Mo in both the bright field (BF) and dark field (DF) images, so that these images cannot be used for the comparison. In the EDX maps (Fig. 5) the HfO_2 layers are uniform and the O and the Hf signal follow each other closely in most of the areas - just as for the Al_2O_3 layers. Again, the metal and O signals are smeared out or interrupted locally. Assuming that the HfO_2 layer is continuous, the smearing out and interruptions must stem from surface roughness effects. Therefore, we conclude that the existence of physical holes can neither be confirmed nor contradicted by the TEM results in any of the samples.

Interestingly, a Ga-rich phase formed in some regions of the HfO_2-CIGS interface, as can be seen in the Ga and O map in Fig. 5. Considering the small extension of this phase and the roughness of the underlying Mo film, even line-scans (not shown) do not reveal, if the phase e.g. consists of GaO_x, $CuGaSe_2$ crystals or elemental Ga. The increase of the Ga signal is not aligned with the apparent openings in the HfO_2 passivation layer. Since this layer leads to severe current blocking, it is unlikely that the formation of the Ga rich phase created holes by locally consuming the HfO_2 entirely. For the Al_2O_3 passivated samples, a formation of a Ga rich phase cannot be clearly distinguished due to noise and the surface roughness effects discussed before.

These results are interesting insofar as they are related to the formation of GaO_x on top of i-ZnO electron contacts in superstrate CIGS solar cells [54–56], on top of Al_2O_3 passivated and unpassivated In_2O_3:H hole contacts in bi-facial solar cells [53] and on Al_2O_3 passivated Mo hole contacts in substrate CIGS solar cells [43]. Whereas the formation of GaO_x from In_2O_3:H and ZnO is thermodynamically advantageous, Al_2O_3 or HfO_2 are both stable against the formation of GaO_x at the sample temperature during co-evaporation. In [53] less GaO_x was formed at the contact, if an ALD-Al_2O_3 layer was inserted between the In_2O_3:H contact and the absorber layer. While our previous electron energy loss spectroscopy results [43] indicated a GaO_x formation, such a formation is less likely in the current solar cells.

6. Final discussion

The same effect of NaF on Al_2O_3 might lower the average

passivation quality of the 15NaF6Al sample compared to the 7.5NaF6Al sample and make sufficient conduction through the layer possible. NaF catalyzing a corrosion of the Al_2O_3 layer and creating openings distributed over the area, is an obvious possible effect that increases both the average interface recombination rate and the conduction through the Al_2O_3 layer. Another explanation is that NaF (or Na or F) changes the Al_2O_3 passivation layer chemically and introduces for example trap states as in [57] or a quasi-conduction band consisting of a wide range of defect states as observed in $LaAlO_3$ [58]. These states could then enhance the conductivity through the Al_2O_3 layer. To influence both the conduction and the passivation effectivity, the proposed traps/quasi-conduction band would have to either compensate the negative oxide charge or change the interface trap density to increase interface recombination.

The conduction enhancement and the passivation effect degradation might, however, be caused by two independent effects as well. For example, while openings might be responsible for the conduction, changes in the oxide charge and interface trap density at the oxide-CIGS interface might reduce the passivation effect additionally even in those areas where no openings have been formed. In this case, NaF precursor layers would have a negative effect even on the passivation quality of thick Al_2O_3 layers, which block the current transport completely regardless of a NaF precursor layer. In any case, a span of Al_2O_3 layer thicknesses is to be expected, where conduction is not sufficient, but the passivation quality is compromised by the NaF precursor layer and this thickness region should be avoided if high passivation quality is to be achieved. We cannot exclude that the observed effects of NaF only happen in ALD deposited Al_2O_3, which involves the use of a metal-organic precursor, and not for example in sputtered Al_2O_3. Unfortunately, the current TEM analysis can exclude neither the possibility of chemical changes nor the possibility of holes in the Al_2O_3 layers and the question, if the reduction of the PL intensity and the increase in conduction have different origins remains open. None of the previous studies [43,53] on unpatterned Al_2O_3 rear contact passivation layers could completely exclude chemical changes in the Al_2O_3 by in-diffusion of Na or F either.

Sodium has a positive effect on the bulk properties of CIGS and is commonly supplied during growth by indiffusion from the soda lime glass. As Al_2O_3 layers act as a Na diffusion barrier [21,38], NaF precursor layers have been widely used on Al_2O_3 passivation layers without any intention to make those layers conductive and without any intentions to change the properties of the Al_2O_3/CIGS interface [10,37–40,47]. Only in rare cases have Al_2O_3 rear contact reflection/passivation layers been implemented into CIGS solar cells without any extra Na added [9,21] or NaF being added after CIGS deposition (post-deposition treatment) [21,41]. The electronic properties of Al_2O_3/CIGS interfaces have been investigated without taking the influence of heat-treatment of the Al_2O_3 layer in presence of Na(F) (and Se) into account, namely either by depositing the Al_2O_3 layer on top of the CIGS layer or by not using a NaF precursor [21,26,27,46]. These results have been widely used to explain results on NaF pre-deposition treated CIGS solar cells. The results in this work and in our previous work [43], however, indicate that the electronic properties of the CIGS/Al_2O_3 interface previously derived may need to be readdressed. In contrast, results on HfO_2 might be more widely applicable.

Al_2O_3 rear contact passivated CIGS solar cells have a high potential to achieve high efficiencies, as indicated by the highest PL intensity and thus highest potential gain $\Delta V_{OC,PL} \approx +170$ mV for the 7.5NaF6Al sample. $\Delta V_{OC,PL}$ could probably be even higher considering that we have not optimized the NaF layer thickness to achieve a high PL intensity. A minimum amount of Na(F) could benefit the interface properties. Fortunately, the Al_2O_3 passivation, achieved multiple benefits or ultrathin CIGS solar cells although the NaF supply was not optimized in our samples: apart from the substantial increase in V_{OC} (+120 mV), it also increases the J_{SC} (+7 mA/cm^2) and thus the efficiency significantly (+3% absolute). It also increases the apparent shunt resistance under illumination and decreases the number of strongly shunted cells. Passivation using Al_2O_3 layers with NaF on top might thus be the best choice, if expensive and time-consuming patterning steps are to be avoided. In this case, NaF precursor deposition needs to be used (which does not exclude other additional Na application methods), and a compromise between conductivity through the Al_2O_3 layer, passivation effectiveness of the Al_2O_3 layer and beneficial and detrimental effects of Na on the absorber needs to be found.

Nano-patterned Al_2O_3 layers do not only enable thicker Al_2O_3 layers and thus a slightly higher reflectance of the rear contact, but also make the above optimization easier. If patterning is used, a Na application method that impacts the passivation quality less than NaF precursor deposition can be used. The optimal Na(F) application method and concentration only needs to minimize the negative effect of NaF (or Na or F) on the passivation effectiveness and optimize the Na content in the absorber. However, a compromise between these two parameters might still be necessary. In conclusion, any dependency of Al_2O_3 characteristics on NaF is of disadvantage if the layer is patterned in an extra-fabrication step and that the large passivation potential of Al_2O_3 might never be fully exploited.

The $\Delta V_{OC,PL}$ of the HfO_2 passivated samples is only 5–11 mV smaller than the $\Delta V_{OC,PL}$ of the sample with the highest average PL intensity (7.5NaF6Al) and nearly 60 mV larger than the $\Delta V_{OC,PL}$, of the sample with the highest solar cell efficiency (15NaF6Al). Therefore, we expect a higher V_{OC} and thus efficiency for CIGS solar cells with ultra-thin absorbers with patterned HfO_2 rear contact passivation layers as compared to unpassivated references. As no dependencies of the passivation layer effectiveness and conductivity on NaF have been observed for HfO_2, it is arguably the passivation material of choice, if conduction through the HfO_2 layer is obtained by nano-patterning. Good interface passivation properties are then ensured independently of Na incorporation method and concentration, and no compromise is needed. Conduction through the passivation layer and passivation effectiveness can be optimized by the nano-patterning method, and the Na(F) application can be optimized independently to achieve good electrical absorber properties.

7. Conclusion

Photoluminescence has been used to estimate possible gains in V_{OC} due to unpatterned rear contact passivation layers in solar cells with ultra-thin CIGS absorbers with flat elemental profiles. We demonstrate potential gains of 160 to 170 mV in the case HfO_2 and of Al_2O_3 passivation layers for CIGS absorbers of 215 nm thickness compared to a reference without passivation. An energy conversion efficiency of 8.6% was obtained for corresponding solar cells using Al_2O_3 as the passivation layer, as compared to 5.6% without passivation. Cells with HfO_2 passivation, in contrast, blocked the photocurrent strongly.

Thin (6 nm) HfO_2 and Al_2O_3 rear contact passivation layers respond very differently to the presence of NaF during CIGS co-evaporation. NaF precursor deposition does not only enable conductivity through the Al_2O_3 passivation layers, but it also strongly reduces their otherwise excellent passivation effectiveness. This suggests that the influence of Na and/or F on Al_2O_3 passivation layers needs to be considered when comparing or reporting results on rear contact passivated solar cells and rear contact properties.

Despite degradation of the passivation due to NaF pre-deposition, Al_2O_3 layers can benefit the performance of ultra-thin CIGS solar cells in multiple ways: besides increasing the efficiency substantially, they increase the apparent shunt resistance under illumination and decrease the number of strongly shunted cells. Passivation with Al_2O_3 layers with NaF on top might thus be the best choice, if expensive and time-consuming patterning steps are to be avoided.

On the other hand, no interdependencies of the passivation layer effectiveness and conductivity on NaF were observed for HfO_2 passivation layers. Therefore, HfO_2 can be the rear contact passivation

material of choice if conduction through the HfO_2 layer is ensured by an extra-fabrication step such as nano-patterning. Then, the nano-patterning can be optimized for conduction through the passivation layer and passivation effectiveness, while the Na(F) incorporation can be optimized for the electrical properties of the absorber.

Acknowledgments

We are grateful for input from our colleagues in the Thin Film Solar Cell group at the Ångström laboratory, especially Jes Larsen and Katharina Rudisch, who helped with the photoluminescence measurements, Tobias Törndal for a short discussion of oxide chemistry and Lars Riekehr for the work at the FIB and TEM.

Funding sources

This work was funded by the Swedish Energy Agency, the Strategic Research program STandUP and the Swedish Research Council (grant 621-2014-5599).

Conflict of interest

The authors declare that there is no conflict of interest regarding the publication of this article.

References

[1] T. Negami, S. Nishiwaki, Y. Hashimoto, N. Kohara, Effect of the absorber thickness on performace of Cu(In,Ga)Se_2 solar cells, in: Proc. 2nd WCPEC, Vienna, 1998: pp. 1181–1184.

[2] W.N. Shafarman, R.W. Birkmire, S. Marsillac, M. Marudachalam, N. Orbey, T. Russel, Effect of reduced deposition temperature, time, and thickness on Cu (In,Ga)Se_2 films and devices, Proc. 26th IEEE Photovolt. Spec. Conf., Anaheim, CA, USA, 1997, pp. 331–334, , https://doi.org/10.1109/pvsc.1997.654095.

[3] O. Lundberg, M. Bodegård, J. Malmström, L. Stolt, Influence of the Cu(In,Ga)Se_2 thickness and Ga grading on solar cell performance, Prog. Photovolt. Res. Appl. 11 (2003) 77–88, https://doi.org/10.1002/pip.462.

[4] D. Ledinek, B. Vermang, M. Edoff, Thickness and Ga-content variations in co-evporated CIGS solar cells with flat Ga profile - an electrical characterization, in: 29th Eur. Photovolt. Sol. Energy Conf. Exhib., 2014: pp. 1832–1836.

[5] Z. Jehl, F. Erfurth, N. Naghavi, L. Lombez, I. Gerard, M. Bouttemy, P. Tran-Van, A. Etcheberry, G. Voorwinden, B. Dimmler, W. Wischmann, M. Powalla, J.F. Guillemoles, D. Lincot, Thinning of CIGS solar cells: part II: cell characterizations, Thin Solid Films 519 (2011) 7212–7215, https://doi.org/10.1016/j.tsf.2010.12.224.

[6] G. Yin, A. Steigert, P. Andrae, M. Goebelt, M. Latzel, P. Manley, I. Lauermann, S. Christiansen, M. Schmid, Integration of plasmonic Ag nanoparticles as a back reflector in ultra-thin Cu(In,Ga)Se_2 solar cells, Appl. Surf. Sci. 355 (2015) 800–804, https://doi.org/10.1016/j.apsusc.2015.07.195.

[7] C. Van Lare, G. Yin, A. Polman, M. Schmid, Light coupling and trapping in ultrathin Cu(In,Ga)Se_2 solar cells using dielectric scattering patterns, ACS Nano 9 (2015) 9603–9613, https://doi.org/10.1021/acsnano.5b04091.

[8] M. Schmid, Review on light management by nanostructures in chalcopyrite solar cells, Semicond. Sci. Technol. 32 (2017), https://doi.org/10.1088/1361-6641/aa59ee 043003.

[9] P. Casper, R. Hünig, G. Gomard, O. Kiowski, C. Reitz, U. Lemmer, M. Powalla, M. Hetterich, Optoelectrical improvement of ultra-thin Cu(In,Ga)Se_2 solar cells through microstructured MgF_2 and Al_2O_3 back contact passivation layer, Phys. Status Solidi Rapid Res. Lett. 10 (2016) 376–380, https://doi.org/10.1002/pssr.201600018.

[10] B. Vermang, J.T. Wätjen, V. Fjällström, F. Rostvall, M. Edoff, R. Gunnarsson, I. Pilch, U. Helmersson, R. Kotipalli, F. Henry, D. Flandre, Highly reflective rear surface passivation design for ultra-thin Cu(In,Ga)Se_2 solar cells, Thin Solid Films 582 (2014) 300–303, https://doi.org/10.1016/j.tsf.2014.10.050.

[11] J. Malmström, O. Lundberg, L. Stolt, Potential for light trapping in Cu(In,Ga)Se_2 solar cells, 3rd World Conf. Photovolt. Energy Convers. May 11–18, 2003 Osaka, Japan, 2003, pp. 344–347.

[12] J. Keller, F. Gustavsson, L. Stolt, M. Edoff, T. Törndahl, On the beneficial effect of Al_2O_3 front contact passivation in Cu(In,Ga)Se_2 solar cells, Sol. Energy Mater. Sol. Cells 159 (2017) 189–196, https://doi.org/10.1016/j.solmat.2016.09.019.

[13] S. Garud, N. Gampa, T.G. Allen, R. Kotipalli, D. Flandre, M. Batuk, J. Hadermann, M. Meuris, J. Poortmans, A. Smets, B. Vermang, Surface passivation of CIGS solar cells using gallium oxide, Phys. Status Solidi 215 (2018), https://doi.org/10.1002/pssa.201700826 1700826.

[14] A. Cuevas, Y. Wan, D. Yan, C. Samundsett, T. Allen, X. Zhang, J. Cui, J. Bullock, Carrier population control and surface passivation in solar cells, Sol. Energy Mater. Sol. Cells 184 (2018) 38–47, https://doi.org/10.1016/j.solmat.2018.04.026.

[15] A. Cuevas, T. Allen, J. Bullock, Yimao Wan, Yan Di, Xinyu Zhang, Skin care for healthy silicon solar cells, Proc. 42nd IEEE Photovolt. Spec. Conf. IEEE, New Orleans, LA, USA, 2015, pp. 1–6, , https://doi.org/10.1109/PVSC.2015.7356379.

[16] A. Cuevas, D. Yan, Misconceptions and misnomers in solar cells, IEEE J. Photovoltaics 3 (2013) 916–923, https://doi.org/10.1109/JPHOTOV.2013.2238289.

[17] R. Kotipalli, B. Vermang, V. Fjällström, M. Edoff, R. Delamare, D. Flandre, Influence of Ga/(Ga + In) grading on deep-defect states of Cu(In,Ga)Se_2 solar cells, Phys. Status Solidi Rapid Res. Lett. 9 (2015) 157–160, https://doi.org/10.1002/pssr.201510024.

[18] O. Lundberg, M. Edoff, L. Stolt, The effect of Ga-grading in CIGS thin film solar cells, Thin Solid Films 480–481 (2005) 520–525, https://doi.org/10.1016/j.tsf.2004.11.080.

[19] P. Würfel, U. Würfel, Physics of Solar Cells, Wiley-VCH Verlag GmbH, Weinheim, Germany, 2005, https://doi.org/10.1002/9783527618545.

[20] U. Würfel, A. Cuevas, P. Würfel, Charge carrier separation in solar cells, IEEE J. Photovoltaics 5 (2015) 461–469, https://doi.org/10.1109/JPHOTOV.2014.2363550.

[21] F. Mollica, J. Goffard, M. Jubault, F. Donsanti, S. Collin, A. Cattoni, L. Lombez, N. Naghavi, Comparative study of patterned TiO_2 and Al_2O_3 layers as passivated back-contact for ultra-thin Cu(In,Ga)Se_2 solar cells, 43rd IEEE Photovolt, Spec. Conf. (2016) 2213–2217, https://doi.org/10.1109/PVSC.2016.7750028.

[22] E. Jarzembowski, B. Fuhrmann, H. Leipner, W. Fränzel, R. Scheer, Ultrathin Cu (In,Ga)Se_2solar cells with point-like back contact in experiment and simulation, Thin Solid Films 633 (2017) 61–65, https://doi.org/10.1016/j.tsf.2016.11.003.

[23] G. Yin, M. Song, S. Duan, P. Manley, D. Greiner, C.A. Kaufmann, M. Schmid, Well-controlled dielectric nanomeshes by colloidal nanosphere lithography for optoelectronic enhancement of ultrathin Cu(In,Ga)Se_2 solar cells, ACS Appl. Mater. Interfaces 8 (2016) 31646–31652, https://doi.org/10.1021/acsami.6b10135.

[24] W. Ohm, W. Riedel, Ü. Askünger, M.D. Heinemann, C.A. Kaufmann, J.L. Garcia, V. Izquierdo, X. Fontané, T. Goislard, M.C. Lux-Steiner, S. Gledhill, An overview of technological aspects of Cu(In,Ga)Se_2 solar cell architectures incorporating ZnO nanorod arrays, Phys. Status Solidi 212 (2015) 76–87, https://doi.org/10.1002/pssa.201431230.

[25] J.M.V. Cunha, P.A. Fernandes, A. Hultqvist, J.P. Teixeira, S. Bose, B. Vermang, S. Garud, D. Buldu, J. Gaspar, M. Edoff, J.P. Leitao, P.M.P. Salome, Insulator materials for Interface passivation of Cu(In,Ga)Se_2Thin films, IEEE J. Photovoltaics 8 (2018) 1313–1319, https://doi.org/10.1109/JPHOTOV.2018.2846674.

[26] R. Kotipalli, B. Vermang, J. Joel, R. Rajkumar, M. Edoff, D. Flandre, Investigating the electronic properties of Al_2O_3/Cu(In,Ga)Se_2 interface, AIP Adv. 5 (2015), https://doi.org/10.1063/1.4932512 107101.

[27] W.-W. Hsu, J.Y. Chen, T.-H. Cheng, S.C. Lu, W.-S. Ho, Y.-Y. Chen, Y.-J. Chien, C.W. Liu, Surface passivation of Cu(In,Ga)Se_2 using atomic layer deposited Al_2O_3, Appl. Phys. Lett. 100 (2012), https://doi.org/10.1063/1.3675849 023508.

[28] A. Morato, B. Vermang, H. Goverde, E. Cornagliotti, G. Meneghesso, J. John, J. Poortmans, Electrical characterization of ALD Al_2O_3 - HfO_2 and PECVD Al_2O_3 passivation layers for p-type CZ-Silicon PERC solar cells, 38th IEEE Photovolt. Spec. Conf, IEEE, 2012, pp. 001077–001082, , https://doi.org/10.1109/PVSC.2012.6317790.

[29] T. Tachibana, T. Sameshima, Y. Iwashita, Y. Kiyota, T. Chikyow, H. Yoshida, K. Arafune, S.I. Satoh, A. Ogura, Material research on high-quality passivation layers with controlled fixed charge for crystalline silicon solar cells, Jpn. J. Appl. Phys. 50 (2011) 04DP09-1–04DP09-4, https://doi.org/10.1143/JJAP.50.04DP09.

[30] J. Cui, Y. Wan, Y. Cui, Y. Chen, P. Verlinden, A. Cuevas, Highly effective electronic passivation of silicon surfaces by atomic layer deposited hafnium oxide, Appl. Phys. Lett. 110 (2017) 021602-1–021602-5, https://doi.org/10.1063/1.4973988.

[31] J. Cui, S.P. Phang, H.C. Sio, Y. Wan, Y. Chen, P. Verlinden, A. Cuevas, Passivation of phosphorus diffused black multi-crystalline silicon by hafnium oxide, Phys. Status Solidi Rapid Res. Lett. 11 (2017), https://doi.org/10.1002/pssr.201700296 1700296.

[32] X. Cheng, P. Repo, H. Halvard, A.P. Perros, E.S. Marstein, M. Di Sabatino, H. Savin, Surface passivation properties of HfO_2 thin film on n-type crystalline Si, IEEE J. Photovoltaics 7 (2017) 479–485, https://doi.org/10.1109/JPHOTOV.2016.2645399.

[33] E. Polydorou, M. Botzakaki, C. Drivas, K. Seintis, I. Sakellis, A. Soultati, A. Kaltzoglou, T. Speliotis, M. Fakis, L.C. Palilis, S. Kennou, A. Fakharuddin, L. Schmidt-Mende, D. Davazoglou, P. Falaras, P. Argitis, C.A. Krontiras, S.N. Georga, M. Vasilopoulou, Insights into the passivation effect of atomic layer deposited hafnium oxide for efficiency and stability enhancement in organic solar cells, J. Mater. Chem. C 6 (2018) 8051–8059, https://doi.org/10.1039/c8tc02243g.

[34] J.T. Gaskins, P.E. Hopkins, D.R. Merrill, S.R. Bauers, E. Hadland, D.C. Johnson, D. Koh, J.H. Yum, S. Banerjee, B.J. Nordell, M.M. Paquette, A.N. Caruso, W.A. Lanford, P. Henry, L. Ross, H. Li, L. Li, M. French, A.M. Rudolph, S.W. King, Review—investigation and review of the thermal, mechanical, electrical, optical, and structural properties of atomic layer deposited high-*k* dielectrics: beryllium oxide, aluminum oxide, hafnium oxide, and aluminum nitride, ECS J. Solid State Sci. Technol. 6 (2017) N189–N208, https://doi.org/10.1149/2.0091710jss.

[35] H.Y. Yu, M.F. Li, D.L. Kwong, ALD $(HfO_2)_x(Al_2O_3)_{1-x}$ high-k gate dielectrics for advanced MOS devices application, Thin Solid Films 462–463 (2004) 110–113, https://doi.org/10.1016/j.tsf.2004.05.010.

[36] S. Bose, J.M.V. Cunha, S. Suresh, D. Wild de, T.S. Lopes, J.R.S. Barbosa, R. Silva, J. Borme, P.A. Fernandes, B. Vermang, P.M.P. Salomé, Optical lithography patterning of SiO_2 layers for interface passivation of thin film solar cells, Sol. RRL 11 (12) (2018), https://doi.org/10.1002/solr.201800212 1800212.

[37] B. Vermang, V. Fjällström, J. Pettersson, P. Salomé, M. Edoff, Development of rear surface passivated Cu(In,Ga)Se_2 thin film solar cells with nano-sized local rear point

contacts, Sol. Energy Mater. Sol. Cells 117 (2013) 505–511, https://doi.org/10.1016/j.solmat.2013.07.025.
[38] B. Vermang, V. Fjallström, X. Gao, M. Edoff, Improved rear surface passivation of Cu(In,Ga)Se_2 solar cells: a combination of an Al_2O_3 rear surface passivation layer and nanosized local rear point contacts, IEEE J. Photovoltaics 4 (2014) 486–492, https://doi.org/10.1109/JPHOTOV.2013.2287769.
[39] B. Vermang, J.T. Wätjen, V. Fjällström, F. Rostvall, M. Edoff, R. Kotipalli, F. Henry, D. Flandre, Employing CIGS solar cell technology to increase efficiency of ultra-thin Cu(In,Ga)Se_2 solar cells, Prog. Photovolt. Res. Appl. 22 (2014) 1023–1029, https://doi.org/10.1002/pip.2527.
[40] B. Vermang, J.T. Wätjen, C. Frisk, V. Fjällstrom, F. Rostvall, M. Edoff, P. Salome, J. Borme, N. Nicoara, S. Sadewasser, Introduction of Si PERC rear contacting design to boost efficiency of Cu(In,Ga)Se_2 solar cells, IEEE J. Photovoltaics 4 (2014) 1644–1649, https://doi.org/10.1109/JPHOTOV.2014.2350696.
[41] D. Ledinek, P. Salome, C. Hägglund, U. Zimmermann, M. Edoff, Rear contact passivation for high band gap Cu(In,Ga)Se_2 solar cells with a flat Ga profile, IEEE J. Photovoltaics 8 (2018) 864–870, https://doi.org/10.1109/JPHOTOV.2018.2813259.
[42] W. Ohm, W. Riedel, U. Aksunger, D. Greiner, C.A. Kaufmann, M.C. Lux-Steiner, S. Gledhill, Bifacial Cu(In,Ga)Se_2 solar cells with submicron absorber thickness: back-contact passivation and light management, IEEE 42nd Photovolt. Spec. Conf, IEEE, 2015, pp. 1–5, , https://doi.org/10.1109/PVSC.2015.7356416.
[43] D. Ledinek, O. Donzel-Gargand, M. Sköld, J. Keller, M. Edoff, Effect of different Na supply methods on thin Cu(In,Ga)Se2 solar cells with Al_2O_3 rear passivation layers, Sol. Energy Mater. Sol. Cells 187 (2018) 160–169, https://doi.org/10.1016/j.solmat.2018.07.017.
[44] Y.S. Lee, T. Gershon, T.K. Todorov, W. Wang, M.T. Winkler, M. Hopstaken, O. Gunawan, J. Kim, Atomic layer deposited aluminum oxide for Interface passivation of $Cu_2ZnSn(S,Se)_4$ thin-film solar cells, Adv. Energy Mater. 6 (2016), https://doi.org/10.1002/aenm.201600198 1600198.
[45] S. Luo, C. Eisler, T.H. Wong, H. Xiao, C.E. Lin, T.T. Wu, C.H. Shen, J.M. Shieh, C.C. Tsai, C.W. Liu, H.A. Atwater, W.A. Goddard, J.H. Lee, J.R. Greer, Suppression of surface recombination in $CuInSe_2$ (CIS) thin films via Trioctylphosphine Sulfide (TOP:S) surface passivation, Acta Mater. 106 (2016) 171–181, https://doi.org/10.1016/j.actamat.2016.01.021.
[46] J. Joel, B. Vermang, J. Larsen, O. Donzel-Gargand, M. Edoff, On the assessment of CIGS surface passivation by photoluminescence, Phys. Status Solidi Rapid Res. Lett. 9 (2015) 288–292, https://doi.org/10.1002/pssr.201510081.
[47] P.M.P.P. Salomé, B. Vermang, R. Ribeiro-Andrade, J.P. Teixeira, J.M.V. Cunha, M.J. Mendes, S. Haque, J. Borme, H. Águas, E. Fortunato, R. Martins, J.C. González, J.P. Leitão, P.A. Fernandes, M. Edoff, S. Sadewasser, Passivation of interfaces in thin film solar cells: understanding the effects of a nanostructured rear point contact layer, Adv. Mater. Interfaces 1701101 (2017) 1–10, https://doi.org/10.1002/admi.201701101.
[48] W.K. Metzger, I.L. Repins, M. Romero, P. Dippo, M. Contreras, R. Noufi, D. Levi, Recombination kinetics and stability in polycrystalline Cu(In,Ga)Se_2 solar cells, Thin Solid Films 517 (2009) 2360–2364, https://doi.org/10.1016/j.tsf.2008.11.050.
[49] K. Kukli, T. Pilvi, M. Ritala, T. Sajavaara, J. Lu, M. Leskelä, Atomic layer deposition of hafnium dioxide thin films from hafnium tetrakis(dimethylamide) and water, Thin Solid Films 491 (2005) 328–338, https://doi.org/10.1016/j.tsf.2005.05.050.
[50] P. Szaniawski, J. Olsson, C. Frisk, V. Fjallstrom, D. Ledinek, F. Larsson, U. Zimmermann, M. Edoff, A systematic study of light-on-bias behavior in Cu(In,Ga)Se_2 solar cells with varying absorber compositions, IEEE J. Photovoltaics 7 (2017) 882–891, https://doi.org/10.1109/JPHOTOV.2017.2655148.
[51] R. Kotipalli, O. Poncelet, G. Li, Y. Zeng, L.A. Francis, B. Vermang, D. Flandre, Addressing the impact of rear surface passivation mechanisms on ultra-thin Cu(In,Ga)Se_2 solar cell performances using SCAPS 1-D model, Sol. Energy 157 (2017) 603–613, https://doi.org/10.1016/j.solener.2017.08.055.
[52] P. Salomé, V. Fjällström, A. Hultqvist, M. Edoff, Na doping of CIGS solar cells using low sodium-doped Mo layer, IEEE J. Photovoltaics 3 (2013) 509–513, https://doi.org/10.1109/JPHOTOV.2012.2226144.
[53] J. Keller, N. Shariati Nilsson, A. Aijaz, L. Riekehr, T. Kubart, M. Edoff, T. Törndahl, Using hydrogen-doped In_2O_3 films as a transparent back contact in (Ag,Cu)(In,Ga)Se_2 solar cells, Prog. Photovolt. Res. Appl. 26 (2018) 159–170, https://doi.org/10.1002/pip.2977.
[54] M.D. Heinemann, D. Greiner, T. Unold, R. Klenk, H.W. Schock, R. Schlatmann, C.A. Kaufmann, The importance of sodium control in CIGSe superstrate solar cells, IEEE J. Photovoltaics 5 (2015) 378–381, https://doi.org/10.1109/JPHOTOV.2014.2360332.
[55] M.D. Heinemann, J. Berry, G. Teeter, T. Unold, D. Ginley, Oxygen deficiency and Sn doping of amorphous Ga_2O_3, Appl. Phys. Lett. 108 (2) (2016), https://doi.org/10.1063/1.4938473 022107.
[56] M.D. Heinemann, V. Efimova, R. Klenk, B. Hoepfner, M. Wollgarten, T. Unold, H.-W. Schock, C.A. Kaufmann, Cu(In,Gas)Se_2 superstrate solar cells: prospects and limitations, Prog. Photovolt. Res. Appl. 23 (2015) 1228–1237, https://doi.org/10.1002/pip.2536.
[57] C. Jin, H. Lu, Y. Zhang, Y. Zhang, H. Guan, L. Wu, B. Lu, C. Liu, Transport mechanisms of leakage current in Al_2O_3/InAlAs MOS capacitors, Solid State Electron. 123 (2016) 106–110, https://doi.org/10.1016/j.sse.2016.06.006.
[58] Z.Q. Liu, D.P. Leusink, W.M. Lü, X. Wang, X.P. Yang, K. Gopinadhan, Y.T. Lin, A. Annadi, Y.L. Zhao, A.R. Barman, S. Dhar, Y.P. Feng, H.B. Su, G. Xiong, T. Venkatesan, Ariando, Reversible metal-insulator transition in $LaAlO_3$ thin films mediated by intragap defects: an alternative mechanism for resistive switching, Phys. Rev. B 84 (2011) 165106. doi:https://doi.org/10.1103/PhysRevB.84.165106.